CHEMISTRY OF MATERIALS
Article

Chem. Mater. **2010,** *22,* 4563–4571 4563
DOI:10.1021/cm100415m

Molecular Heterobimetallic Approach to Li-Containing MgO Nanoparticles with Variable Li-Concentrations Using Lithium-Methylmagnesium Alkoxide Clusters

Stephan Heitz, Jan-Dirk Epping, Yilmaz Aksu, and Matthias Driess*

Institute of Chemistry, Metalorganics and Inorganic Materials, Technische Universität Berlin, Strasse des 17. Juni 135, Sekr. C2, D-10623 Berlin, Germany,

Received February 9, 2010. Revised Manuscript Received June 18, 2010

Facile synthesis and characterization of the first heterobimetallic lithium-methylmagnesium-alkoxide clusters [Li(thf)(MeMg)$_3$(μ_3-OR)$_4$] (R = ^{i}Pr (**1a**), ^{t}Bu (**1b**), ^{Cy}Hex (**1c**)) having a cubane-shaped $LiMg_3O_4$ core is reported. They have been employed as molecular single-source precursors for "bottom up" synthesis of Li-containing MgO nanoparticles with varying Li-concentrations. This can be achieved by solid state decomposition of homogeneous mixtures of the latter compounds (**1a**−**c**) with the corresponding homometallic alkylmagnesium alkoxide cubanes [MeMg(μ_3-OR)]$_4$ (R = ^{i}Pr (**2a**), ^{t}Bu (**2b**), ^{Cy}Hex (**2c**)). Characterization of the final obtained materials was accomplished by a combination of different analytical techniques such as TGA, PXRD, TEM, Raman spectroscopy, ^{7}Li MAS NMR spectroscopy, elemental analysis, and nitrogen adsorption. The different parameters that affect the composition and morphology of the Li-containing MgO nanoparticles have been examined. It has been found that Li concentrations up to 1 wt % lead to well-defined crystalline materials, where the Li ions are likely incorporated in the magnesium oxide lattice, whereas higher Li concentrations afford less-ordered materials, which consist of additional crystalline and amorphous phases.

Introduction

Because of the massively increased consumption of world oil reserves, the research for suitable alternative sources of organic bulk chemicals has shaped up as one of the major challenges in modern chemistry.[1] The considerable natural gas reserves worldwide turn methane to the most promising candidate and its oxidative coupling with oxygen (oxidative coupling of methane, OCM) over heterogeneous catalysts to ethylene hallmarks the latter to be a highly valuable reaction for the petrochemical industry.

Lithium-doped MgO systems, which were described the first time in 1985 by Lunsford et al.,[2,3] are promising catalyst for OCM. Lunsford and co-workers proposed a mechanism, in which the replacement of Mg^{2+} by Li^+ ions in the MgO lattice leads to [Li^+O^-]-centers, which are believed to serve as active sites in the catalytic process. The initial step of the reaction may involve homolytic C−H activation of methane on the O^- radical anion centers. Thus, methyl radicals are formed,[4] which undergo subsequent coupling in the gas phase to give ethane and further related conversion to ethylene.[5] By comparing pure Li_2CO_3 with lithium-doped MgO, Lunsford proposed that the activity of the catalyst strongly depends on the contribution of lithium ions in the MgO lattice.[3] Furthermore, it has been suggested that the Li-ions are uniformly distributed in the MgO lattice at high temperatures, which may explain an increase of catalytic activity with increasing lithium concentrations. In other words, a homogeneous and optimum dispersity of different Li-ion concentrations in the MgO lattice is highly desirable for a proof-of-concept.

Currently, lithium-containing MgO is prepared by thermal treatment of mixtures of magnesium and lithium salts, such as hydroxides, carbonates, nitrates, and acetates.[6a,b] However, this method requires temperatures up to 1000 °C and leads already at low Li concentrations (>1 wt %) to mixtures of Li_2CO_3 and lithium-doped MgO. In contrast, the use of molecular heterobimetallic metalorganic precursors in which all required elements are consistently distributed on the molecular scale can offer a unique and facile approach for the preparation of pure nanoscaled heterobimetallic oxides under gentle conditions.[6c] In fact, decomposition of suitable SSPs can occur at relatively

*Corresponding author. E-mail: matthias.driess@tu-berlin.de.

(1) Lunsford, J. H. *Catal. Today* **2000**, *63*, 165.
(2) Ito, T.; Lunsford, J. H. *Nature* **1985**, *314*, 721.
(3) Ito, T.; Wang, J. X.; Lin, C. H.; Lunsford, J. H. *J. Am. Chem. Soc.* **1985**, *107*, 5062.
(4) (a) Driscoll, D. J.; Martir, W.; Wang, J. X.; Lunsford, J. H. *J. Am. Chem. Soc.* **1985**, *107*, 58. (b) Driscoll, D. J.; Lunsford, J. H. *J. Phys. Chem.* **1985**, *89*, 4415.
(5) Campbell, K. D.; Morales, E.; Lunsford, J. H. *J. Am. Chem. Soc.* **1987**, *109*, 7900.
(6) (a) Camino, J. I.; Holgado, M. J.; Rives, V. *React. Kinet. Catal. Lett.* **1991**, *44*(2), 469. (b) Choudhary, V. R.; Mulla, S. A. R.; Pandit, M. Y.; Chaudhari, S. T.; Rane, V. H. *J. Chem. Technol. Biotechnol.* **2000**, *75*, 828. (c) Aksu, Y.; Driess, M. *Angew. Chem., Int. Ed.* **2009**, *121*, 7918.

Published on Web 07/20/2010

low temperature to give the desired material with optimum dispersity of both metals. The advantage of the latter method over a multicomponent approach has recently been demonstrated for the preparation of several functional heterobimetallic zinc oxide materials[7] and has even paved the way to novel tin-rich indium tin oxide (ITO) materials.[6c] For example, heterobimetallic alkali metal-methylzinc alkoxides clusters[7] with a MZn_3O_4 cubane shaped core (M = Li, Na, K) can be considered as a structural cutout of the corresponding M−ZnO lattice, and thus, such heterobimetallic systems turned out to be excellent SSPs for the synthesis of alkali metal-doped ZnO nanoparticles.[8] Accordingly, heterobimetallic lithium-methylmagnesium-alkoxide analogues of the MZn_3O_4 cubanes could be suitable SSPs for the preparation of lithium-containing MgO. Several heterobimetallic Li−Mg-compounds are described in literature, which seem to be suitable precursors for the preparation of lithium doped MgO as well.[9] However, to the best of our knowledge, no decomposition of any of these compounds has been reported as yet. We herein describe the synthesis and structural characterization of the first Li/Mg-heterobimetallic alkyl alkoxide SSPs with a $LiMg_3O_4$ core and their thermal decomposition in solid state. Furthermore, decomposition of mixtures of the $LiMg_3O_4$ SSPs with related molecular, homometallic Mg_4O_4 clusters as MgO SSPs enables the formation of lithium-containing MgO nanoparticles with *variable* Li-concentrations.

Results and Discussion

Heterobimetallic lithium-methylmagnesium-alkoxides $[Li(thf)(MeMg)_3(\mu_3\text{-}OR)_4]$ [R = ^{i}Pr (**1a**), ^{t}Bu (**1b**), ^{Cy}Hex (**1c**)] are surprisingly easily accessible by scrambling reaction of tetrameric alkylmagnesium alkoxide cubanes $[MeMg(\mu_3\text{-}OR)]_4$ [R = ^{i}Pr (**2a**), ^{t}Bu (**2b**), ^{Cy}Hex (**2c**)][10] with the corresponding lithium alkoxides (LiOR)[11] in tetrahydrofuran (THF) at ambient temperature (Scheme 1). They can be isolated as colorless crystals in 78% (**1a**), 77% (**1b**), and 93% yield (**1c**), respectively. In addition, small amounts of insoluble byproducts could be obtained that have been separated by filtration of the crude reaction mixtures. The byproducts are likely polymeric or oligomeric species, formed by coordination of THF to magnesium.[12]

Scheme 1. Synthesis of 1a−c by Scrambling Reaction of 2a, 2b, and 2c with the Corresponding Lithium Alkoxides

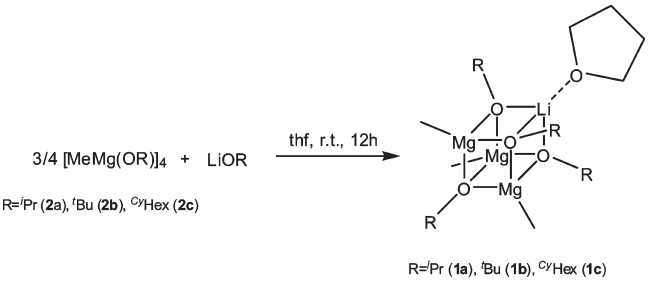

The compounds **1a−c** are soluble in polar solvents, such as THF and related ethers but are, in contrast to the homometallic alkylmagnesium alkoxide cubanes, only sparingly soluble in nonpolar solvents, such as hexane and toluene. This is probably because of the more ionic character of the heteroaggregate by the presence of lithium. All synthesized compounds are very sensitive toward moisture and oxygen. The compositions of **1a−c** are in accordance with the respective ^{1}H and $^{13}C\{^{1}H\}$ NMR spectroscopic data. Figure 1 depicts the $^{13}C\{^{1}H\}$ NMR spectra for all prepared compounds in C_6D_6 solutions. The latter show the expected resonance signals without presence of a degradation or redistribution product.[10,12] Two sets of resonances are visible in all spectra because of the four substituent groups (−R) three are chemically equivalent. Apparently, variation of the alkoxide group has an influence on the chemical shift of the methyl groups of the MgMe moieties, which lies between δ = −14.3 (**1c**) and −11.8 (**1b**) ppm.

Solid-state CPMAS (cross-polarization magic angle spinning) NMR measurements were performed on all prepared compounds. Figure 2 shows as an example the $^{13}C\{^{1}H\}$ and ^{7}Li NMR spectra of **1a** in C_6D_6 versus in the solid state. The spectra exhibit close similarity in both states and thus show that the heterocubane structure is retained in solution. The relatively narrow signal in the solid-state ^{7}Li NMR spectrum confirms the high crystallinity of the sample. Small deviations of the chemical shift in the solid-state versus solution spectra can be explained by intermolecular interactions between the closely packed molecules.

In contrast, dissolution of **1a−c** in polar solvents such as THF causes dissociation processes. Thus, solution of **1a** in d^8-THF reveal two resonance signals in the ^{7}Li NMR spectrum (Figure 3). At the same time, only one set of signals for the ^{i}Pr groups results in the ^{13}C NMR spectrum. The equilibrium can be shifted back to the undissociated $LiMg_3O_4$ heterocubane in nonpolar solvents. Likewise, evaporation of THF solutions of **1a** in vacuo and redissolution in C_6D_6 reproduces predominantly

(7) (a) Merz, K.; Block, S.; Schoenen, R.; Driess, M. *Dalton Trans.* **2003**, 3365. (b) Polarz, S.; Orlov, A. V.; van den Berg, M. W. E.; Driess, M. *Angew. Chem., Int. Ed.* **2005**, *44*, 7892. (c) Arndt, S.; Aksu, Y.; Driess, M.; Schomäcker, R. *Catal. Lett.* **2009**, *131*, 258.

(8) (a) Jana, S.; Aksu, Y.; Driess, M. *Dalton Trans.* **2009**, 1516. (b) S. Polarz, S; Orlov, A.; Hoffmann, A.; Wagner, M. R.; Rauch, C.; Kirste, R.; Gehlhoff, W.; Aksu, Y.; Driess, M.; van den Berg, M. W. E.; Lehmann, M. *Chem. Mater.* **2009**, *21*(16), 3889. (c) Rauch, C.; Gehlhoff, W.; Wagner, M. R.; Malguth, E.; Callsen, G.; Kirste, R.; Salameh, B.; Hoffmann, A.; Polarz, S.; Aksu, Y.; Driess, M. *J. Appl. Phys.* **2010**, *107*, 024311.

(9) (a) Henderson, K. W.; Mulvey, R. E.; Reinhard, F. B. M. *J. Am. Chem. Soc.* **1994**, *116*, 10777. (b) Antolini, F.; Hitchcock, P. B.; Lappert, M. F.; Wei, X.-H. *Organometallics* **2003**, *22*, 2505. (c) Hsueh, M.-L.; Ko, B.-T.; Athar, T.; Lin, C.-C.; Wu, T.-M.; Hsu, S.-F. *Organometallics* **2006**, *25*, 4144. (d) Zuniga, M. F.; Kreutzer, J.; Teng, W.; Ruhlandt-Senge, K. *Inorg. Chem.* **2007**, *46*, 10400.

(10) (a) Heitz, S.; Aksu, Y.; Merschjann, C.; Driess, M. *Chem. Mater.* **2010**, *22*, 1376. (b) Sung, M. M.; Kim, C. G.; Kim, J.; Kim, Y. *Chem. Mater.* **2002**, *14*, 826.

(11) (a) Kamienski, C. W.; Lewis, D. H. *J. Org. Chem.* **1965**, *30*, 3498. (b) Lochmann, L.; Pospisil, J.; Vodnansky, J.; Trekoval, J.; Lim, D. *Collect. Czech. Chem. Commun.* **1965**, *30*, 2187. (c) Lochmann, L.; Coupek, J.; Lim, D. *Collect. Czech. Chem. Commun.* **1970**, *35*, 733.

(12) Ashby, E. C.; Nackashi, J.; Parris, G. E. *J. Am. Chem. Soc.* **1975**, *97* (11), 3162.

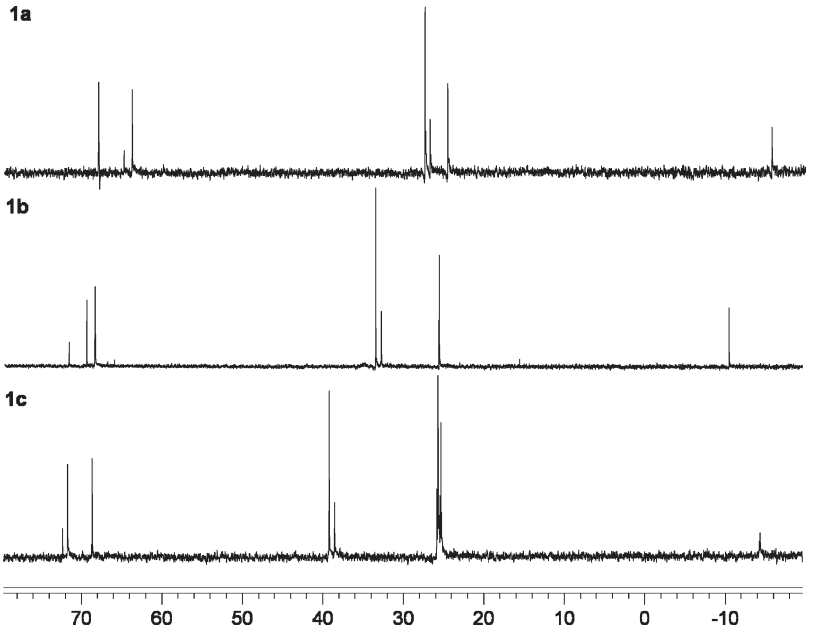

Figure 1. $^{13}C\{^1H\}$ NMR spectra (200 MHz) of **1a**−**c** in C_6D_6 at room temperature.

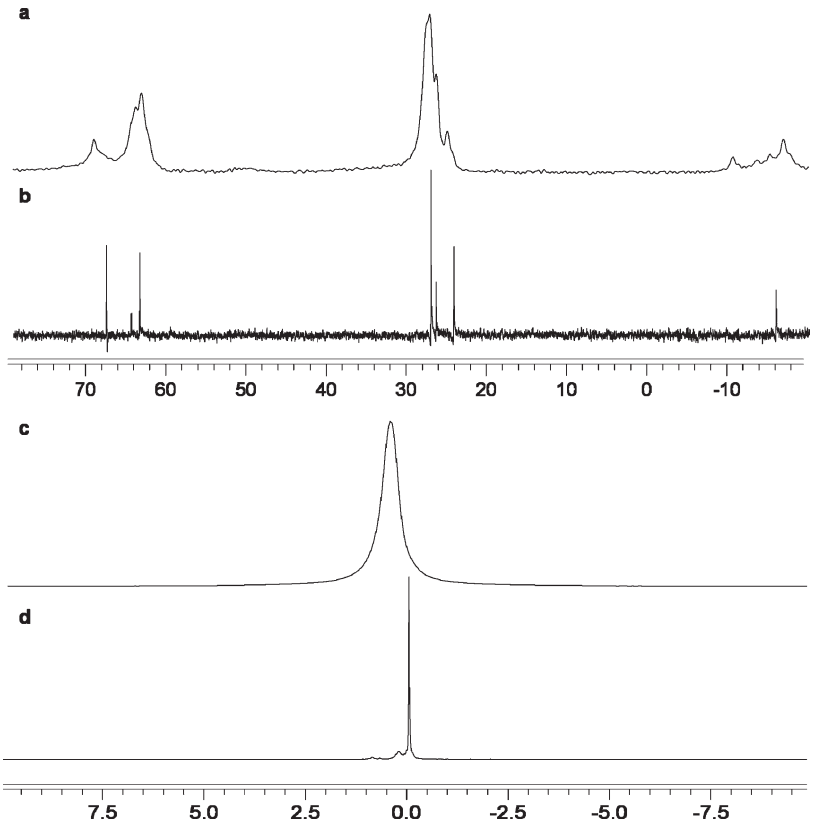

Figure 2. (a) $^{13}C\{^1H\}$ MAS NMR spectrum of **1a**; (b) $^{13}C\{^1H\}$ NMR spectrum of **1a** in C_6D_6; (c) $^{7}Li\{^1H\}$ MAS NMR spectrum of **1a**; (d) $^{7}Li\{^1H\}$-NMR spectrum of **1a** in C_6D_6.

undissociated **1a** as shown by ^1H and ^{13}C NMR spectroscopy (Figure 2). ^7Li NMR (Figure 2d) shows that only a very small fraction of dissociated byproduct (resonance at 0.2 ppm) is present under these conditions. Deviations of the elemental analyses result from the expected values (see Experimental Section) are presumably because of the high sensitivity of the compounds toward moisture and air. The tendency of **1a**−**c** to undergo facile dissociation in ethereal (coordinating) solvents is similar to that observed for oligomeric alkylmagnesium alkoxides.[12]

Single-crystals of [Li(thf)(MeMg)(μ_3-O^{Cy}Hex)$_4$] **1c** suitable for X-ray diffraction analysis could be obtained by crystallization in a 1:1 mixture of hexane and THF. The compound crystallizes in the orthorhombic space group $Pca2_1$. The molecular structure of **1c** determined from X-ray diffraction analysis is shown in Figure 4, and Table 1

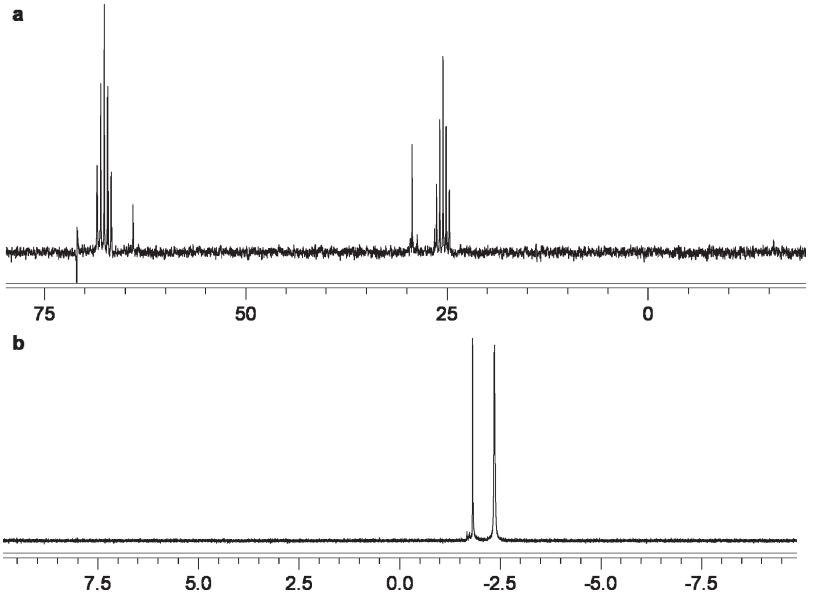

Figure 3. (a) $^{13}C\{^{1}H\}$ NMR spectrum of **1a** in d^8-THF (multiplets are THF resonances); (b) $^{7}Li\{^{1}H\}$ NMR spectrum of **1a** in d^8-THF.

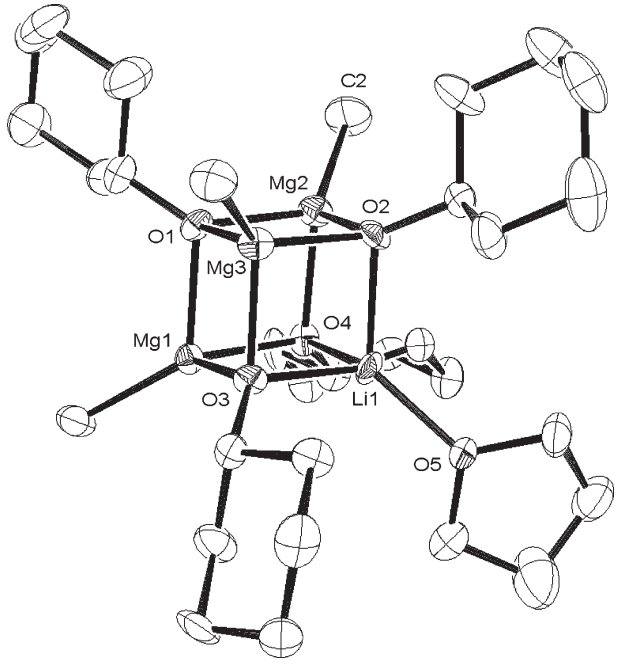

Figure 4. Molecular Structure of $[Li(thf)(MeMg)_3(\mu_3\text{-}O^{Cy}Hex)_4]$ (**1c**). Thermal ellipsoids are drawn at the 50% probability level. The hydrogen atoms are omitted for clarity. For selected distances and angles, see Table 1 and Supporting Information (SI 1).

lists selected bond angles and distances (see also Supporting Information SI 1).

Cluster **1c** consists of a distorted $[LiMg_3O_4]$ framework. Remarkably, the Mg(1)−O(1), Mg(2)−O(1), and Mg(3)−O(1) distances of 2.064(3), 2.069(3), and 2.062(3) Å are significantly longer than the other Mg−O distances of the Mg ions to the O(2), O(3), and O(4) atoms. The latter are directly connected to the "harder" Li ion, which implies a stronger ionic character (Coulomb interaction) of the oxygen centers with the adjacent Mg ions than that of O(1).

Single-crystals of **1a** have also been obtained by crystallization in *n*-hexane at −20 °C. According to an X-ray analysis, **1a** shows similar structural characteristics as **1c**. However, because of the poor single-crystal quality the structure can not be discussed.

Table 1. Selected Bond Distances [Å] and Angles [deg] of 1c

Mg(1)−O(1)	2.064(4)
Mg(2)−O(1)	2.069(3)
Mg(3)−O(1)	2.062(3)
Mg(1)−O(3)	2.013(3)
Mg(1)−O(4)	2.013(3)
Li(1)−O(2)	2.019(9)
Li(1)−O(3)	2.008(8)
Li(1)−O(4)	2.025(7)
Li(1)−O(5)	1.907(8)
O(4)−Mg(1)−O(3)	90.73(13)
O(3)−Mg(3)−O(2)	89.52(14)
O(4)−Mg(1)−O(1)	84.48(13)
O(3)−Mg(1)−O(1)	85.56(13)
O(1)−Mg(1)−Li(1)	85.74(19)
Mg(3)−O(1)−Mg(1)	93.11(12)
Mg(1)−O(4)−Mg(2)	97.22(14)
O(3)−Li(1)−O(2)	90.1(3)
O(5)−Li(1)−O(3)	128.1(4)

Initially, the decomposition behavior of the heterobimetallic lithium-methylmagnesium-alkoxides **1a**−**c** was investigated by TGA-DTG studies using synthetic air (20% O_2, 80% N_2). The respective TGA and DTG curves for **1b** are shown in Figure 5 (see Supporting Information SI 2a,b).

The TGA curve displays a weight loss of 16.25% at the very beginning of the decomposition, which cannot be observed during the decomposition of the corresponding alkylmagnesium alkoxides **2b**.[10] Consequently, the latter mass loss is mostly due to the loss of the relatively volatile THF ligand at lithium, with a theoretical mass loss for THF of 14.73%. The slightly higher mass loss corresponds to concomitantly partial oxidation of the precursor. The main mass loss starts at 150 °C and is finished around 390 °C, which results in a final mass of 28.28%. This value agrees well with the calculated mass for complete degradation to "Li−MgO" (29.39%). The TGA and DTG curves for **1a** and **1c** are similar to those observed

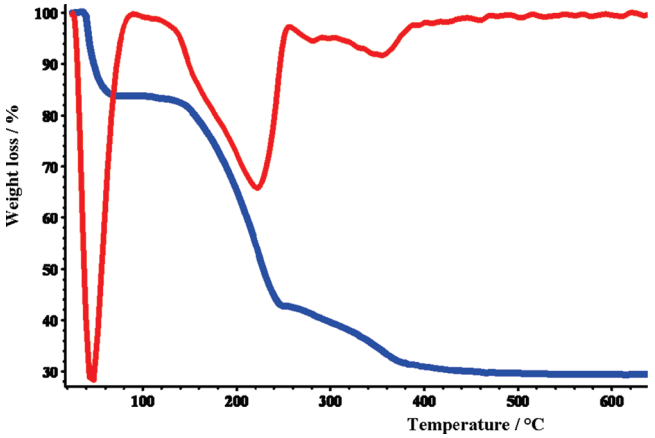

Figure 5. TGA and DTG curves for the degradation of [Li(thf)-(MeMg)$_3$(μ^3-O^{t}Bu)$_4$] (**1b**) in dry synthetic air.

Table 2. Carbon Impurities, Particle Sizes, and BET-Surfaces of Li−MgO Samples with Variable Li Concentrations

wt % Li	carbon impurities (wt %)	particle Size from Debye−Scherrer equation (nm)	lattice constant (Å)	BET-surface (m^2/g)
0.1	0.83	10.92	4.216	92.0
0.5	0.67	12.06	4.213	67.6
1	0.64	14.53	4.212	48.5
2	0.86	32.07	4.211	5.7
3	1.10	32.81	4.211	4.8
4	1.96	25.69	4.211	11.7

for **1b**. However, the complete degradation of **1c** requires higher temperature (500 °C) because of the lower volatility of the cyclohexyl groups in comparison with the *iso*-propoxide and *tert*-butoxide ligands (see Supporting Information SI 2a,b). Investigation of the degradation of **1b** by TGA-MS (see Supporting Information SI 3b) revealed that CH_4 (*m*/*e* 16) and H_2O (*m*/*e* 18) are produced at relatively low temperature (at 80 °C), while THF (*m*/*e* 72) is mostly oxidized under this conditions. Additionally, isobutene (*m*/*e* 56), C_3H_4 (*m*/*e* 40), and CH_4 (*m*/*e* 16) are produced at ~180 °C by decomposition of residual *tert*-butoxide groups (see Supporting Information SI 3b). At around 350 °C, mostly H_2O and CO_2 are formed through complete combustion of the residual organics (see Supporting Information SI 3b).

Monitoring the degradation of **1a** and 1c by TGA-MS reveals similar features. However, degradation of **1a** leads to formation of acetone (*m*/*e* 58) instead of isobutene, which was also observed for the decomposition of related methylzinc isopropoxide clusters.[16]

In the case of **1c**, a predominant formation of H_2O and CO_2 could not be observed before 500 °C. We attribute this to the lower reactivity of the cyclohexyl groups in **1c** that, in fact, leads to materials with a higher amounts of carbon impurities (see Supporting Information SI 3a,c).

In addition, Li-MgO samples with lower lithium amounts (between 0.1 and 4 wt %) were prepared by solid-state decomposition of mixtures of **2b** and **1b** under dry synthetic air in the temperature range of 25−600 °C with a heating rate of 5 K min^{-1}. The concentrations of lithium in the samples were determined by atomic absorption spectroscopy (AAS) (Table 2; see also Supporting Information SI4).

Figure 6 shows the PXRD patterns of Li-doped MgO with 2 wt % Li (Figure 6a) and 4 wt % Li (Figure 6g). Within the detection limit of the applied diffractometer, MgO is the only detectable crystalline phase at Li concentrations up to 2 wt % (Figure 6a, see also Supporting Information SI 5). However, at higher Li concentrations additional reflections appear, which can be assigned to lithium carbonate (Figure 6b). Small amounts of magnesium hydroxide could also be detected in some samples because of partial chemisorption of H_2O by MgO.

The reflex positions were used to calculate the lattice parameter a (Table 2; Figure 7). For comparison, the lattice constant for MgO prepared from pure **1b**[10] was added as well. It is shown in Figure 7 that Li concentrations up to 2 wt % lead to a contraction of the MgO lattice from 4.216 Å down to 4.211 Å. This indicates that Li is initially incorporated into the MgO matrix, since the formation of a separate phase would not affect the lattice constant.

The purity of the samples was determined by IR spectroscopy and elemental analysis (Table 2). The results coincide well with the PXRD investigations. All samples with less than 3 wt % lithium contain low carbon impurities, with one even as low as 0.64 wt % carbon (Table 2). At Li-concentrations higher than 2 wt %, the impurities are increased significantly, resulting in carbon concentrations up to 1.96 wt %. These can be assigned to carbonates, according to the characteristic IR bands between 1300 and 1500 cm^{-1} (see Supporting Information SI 6). Additionally, the IR spectra prove the presence of hydroxo groups at the surface area of the materials, as shown by the vibration bands between 3000 and 3800 cm^{-1}. Since hydroxo groups are stable up to 800 °C,[13] they are still present under the applied decomposition conditions.

The particle sizes were calculated from the half-width of the isolated reflex centered at $2\theta = 42.9°$ and corrected for instrumental broadening using the Debye−Scherrer equation (Table 2). The particle size increases slightly from 10.9−14.5 nm for the lithium-doped magnesium oxide samples with Li concentrations between 0.1 and 1 wt %. The most considerable change can be observed for the samples with Li concentrations between 1 and 2 wt %, where the particle size increases from 14.5 to 32.1 nm. At higher Li concentrations, the particle size is almost constant. These observations indicate that lithium-doped magnesium oxide samples with Li concentrations higher than 1 wt % lead to a phase segregation. Perrichon and Durupty[14] assumed that a lithium phase present at the interface of MgO particles undergoes transformations and acts as a "mineralizer" by inducing a partial dissolution of MgO and thus favoring the growth of larger particles. As already mentioned, Li concentrations lower than 1 wt % led only to a slight change of the particle size.

(13) Bailly, M. L.; Costentin, G.; Pernot, H. L.; Krafft, J. M.; Che, M. *J. Phys. Chem. B* **2005**, *109*, 2404.
(14) Ishikawa, K.; Fujima, N.; Komura, H. *J. Appl. Phys.* **1985**, *57*(3), 973.

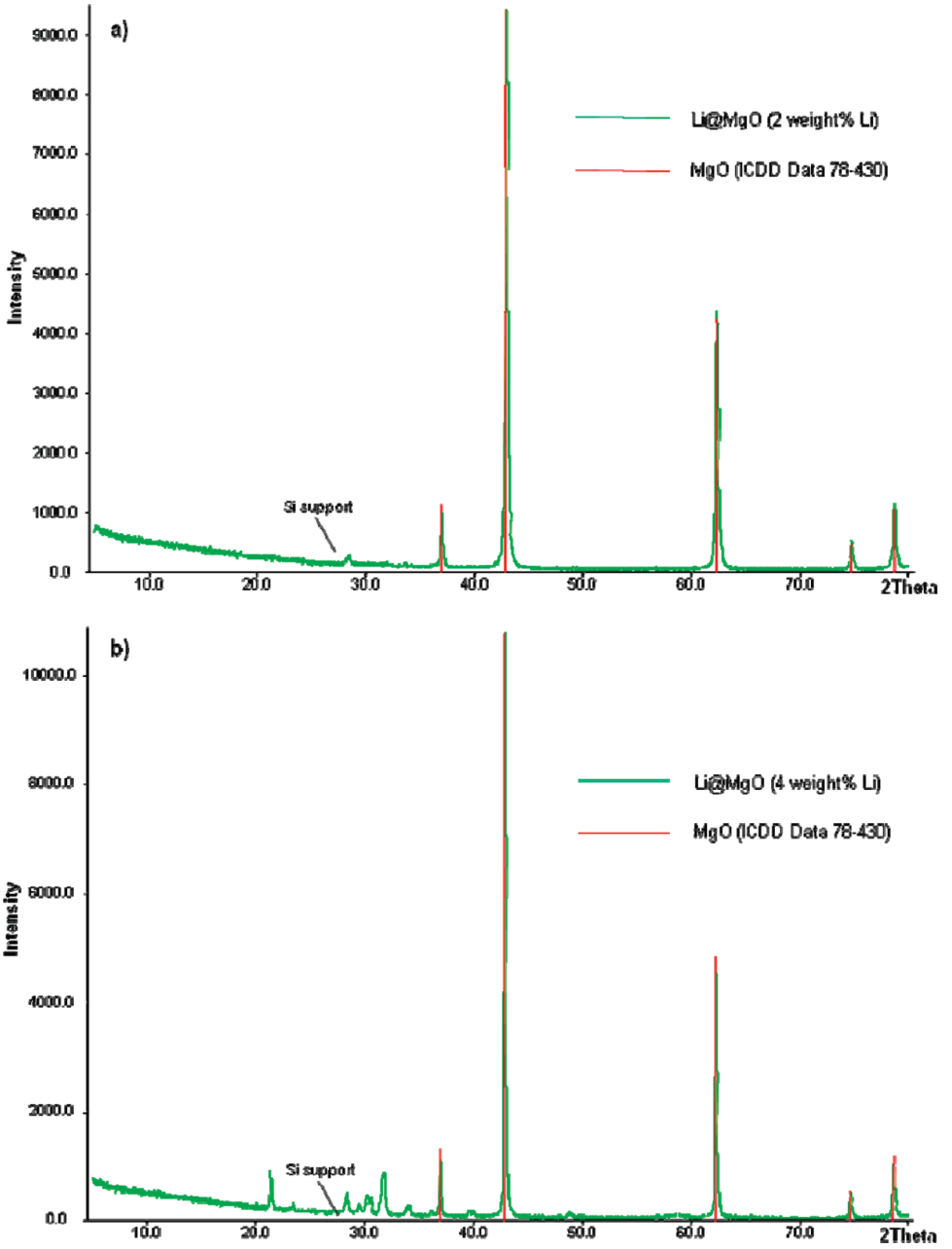

Figure 6. PXRD pattern of lithium doped MgO obtained from mixtures of **1b** and **2b** (20% O_2; 80% N_2; RT → 600 °C (2 h); 5 K min^{-1}): (a) 2 wt % Li; (b) 4 wt % Li.

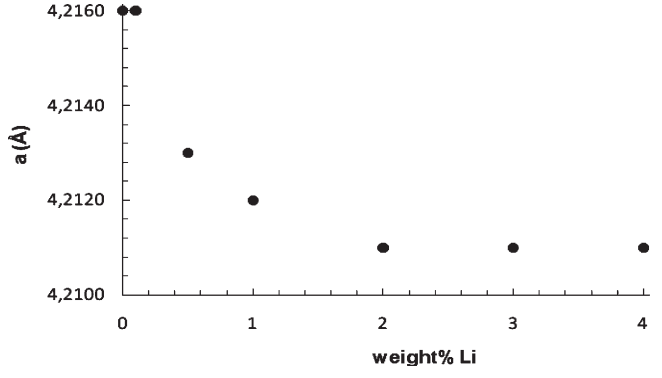

Figure 7. Li content dependence of the lattice constant.

That no phase separation takes place at this concentration range and the Li-ions are well incorporated into the MgO lattice could be particularly useful for further structure−activity investigations on Li-containing MgO in catalysis.

The specific BET (Brunauer−Emmet−Teller) surface areas of all samples were measured using nitrogen adsorption at 77 K (Table 2). According to the particle sizes, the surface areas of the samples decrease with higher Li-concentrations and lie between 92.0 m^2/g for 0.1 wt % Li versus 4.8 m^2/g for 3 wt % Li. The most significant change can be observed going from 1 wt % Li (48.5 m^2/g) to 2 wt % Li (5.7 m^2/g).

The SEM (scanning electron microscopy) images (Figure 8a and b) of all samples show that the lithium-containing MgO samples consist of large agglomerates, which do not significantly change in their morphology depending on the lithium concentration. A better resolution

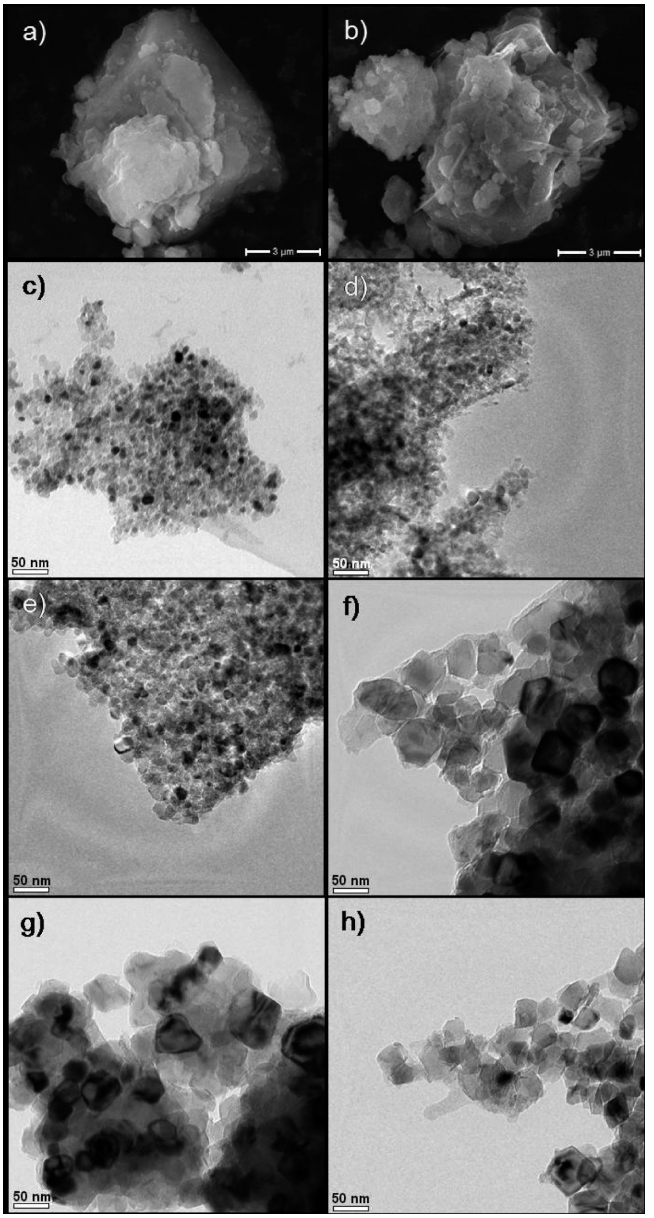

Figure 8. SEM micrographs of lithium-containing MgO prepared from mixtures of **1b** and **2b** (20% O_2; 80% N_2; RT → 600 °C (2 h); 5 K min^{-1}) with (a) 0.1 wt % Li and (b) 4 wt % Li. TEM micrographs of lithium-doped MgO prepared from mixtures of **1b** and **2b** (20% O_2; 80% N_2; RT → 600 °C (2 h); 5 K min^{-1}) with (c) 0.1 wt % Li, (d) 0.5 wt % Li, (e) 1 wt % Li, (f) 2 wt % Li, (g) 3 wt % Li, and (h) 4 wt % Li.

of the agglomerates was achieved using TEM (transmission electron microscopy). Accordingly, the agglomerates consist of a large amount of irregularly shaped nanoparticles (Figure 8c−h). Particles with Li concentrations up to 1 wt % show a similar morphology as undoped MgO prepared from **1a**−**c**[10a] but minor bigger particle sizes. In this range, the particle size increases only slightly with the Li concentration. The most considerable change of morphology and particle size is observed in samples with Li concentrations between 1 and 2 wt %, leading to large and almost spherical particles. Higher Li concentrations do not lead to any further change of morphology or particle size. These observations coincide well with the results by PXRD and BET measurements.

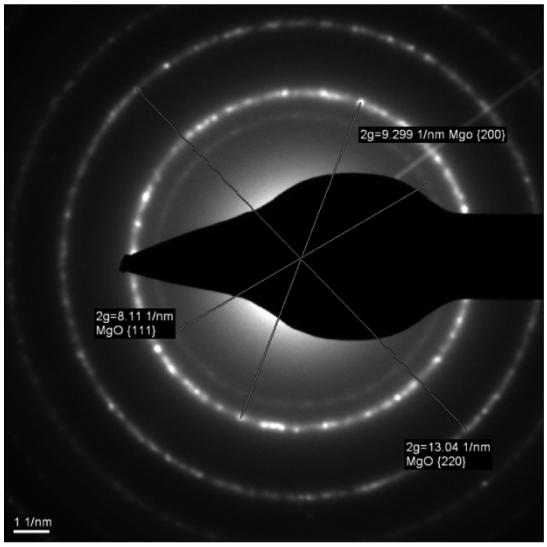

Figure 9. Diffraction pattern of a Li−MgO sample with 1.0 wt % Li.

The presence of diffraction rings at the diffraction pattern of Li−MgO samples with 1.0 wt % Li (Figure 9) prove the crystalline character of the material. The reciprocal lengths of the rings coincide well with MgO (NaCl structure, fcc, a = 0.4212 Å). EDX-measurements (see Supporting Information SI 8) performed on the agglomerates on carbon coated Cu TEM grids showed magnesium and oxygen as the only observable elements in the materials.

Additionally, Raman spectroscopy (see Supporting Information SI 7) was performed on Li-containing MgO samples with different Li-concentrations. Three bands (280, 445, and 1088 cm^{-1}) can be assigned to MgO. The band at 280 cm^{-1} relates to a transverse acoustic phonon, and the band at 445 cm^{-1} can be assigned to a transverse optic phonon modes.[14] The band at 1088 cm^{-1} is probably caused by surface phonon modes, which as usual appear in a transverse optical−longitudinal optical gap.[14,15] Li-concentrations of 2 and 3 wt % give rise to an additional band at 710 cm^{-1}, which could not be assigned as yet.

Solid-state MAS ^{7}Li NMR measurements were performed on as-prepared Li-containing MgO samples using mixtures of the precursors **1b** and **2b** (Figure.10). All materials exhibit one main resonance at −0.1 ppm. The line width of this signal increases with increasing lithium concentrations. Samples with Li concentrations up to 1 wt % show signals with narrow lines, comparable to crystalline Li_2O, which indicates, that the lithium ions are arranged in an ordered crystalline environment. As shown above by PXRD data (Figure 6a), MgO is the only detectable crystalline phase in these materials. This suggests that at relatively low Li-concentrations the Li-ions are incorporated into the MgO lattice. However, samples with 2 or more wt % Li exhibit visibly broader resonances in the ^{7}Li NMR spectrum with a distinct

(15) Böckelmann, H. K.; Schlecht, R. G. *Phys. Rev. B* **1974**, *10*, 5225.
(16) Schröder, D.; Schwarz, H.; Polarz, S.; Driess, M. *Phys. Chem. Chem. Phys.* **2005**, *7*, 1049.

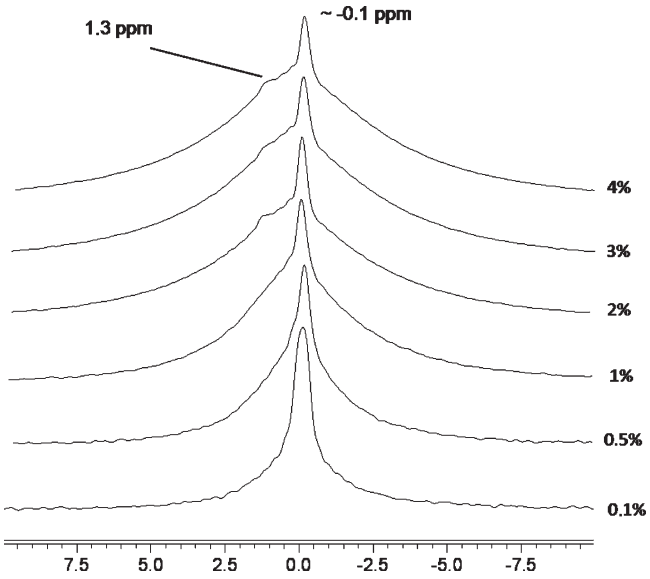

Figure 10. ^{7}Li-MAS NMR spectra of Li-containing MgO samples as-prepared from mixtures of **1b** and **2b** (20% O_2; 80% N_2; RT → 600 °C (2 h); 5 K min^{-1}).

shoulder at 1.3 ppm. For Li concentrations higher than 1 wt %, the occurrence of this broader signal in addition to the sharp signal at −0.1 ppm indicates that some of the Li-ions are now arranged in a more disordered environment, which is typical for amorphous phases.

Conclusions

In conclusion, the first heterobimetallic alkyl alkoxides **1a**−**c** [Li(thf)(MeMg)$_3$(μ^3-OR)$_4$] (R = ^{i}Pr, ^{t}Bu, ^{Cy}Hex) were prepared successfully by interconversion of [MeMg(μ^3-OR)]$_4$ **2a**−**c** with the corresponding lithium alkoxides. Thermal decomposition of homogeneous mixtures consisting of **1a**−**c** and the corresponding homometallic Mg_4O_4 compounds **2a**−**c** in different molar ratios lead to Li-containing MgO with different Li-concentrations. All decompositions of **1b** take place at temperatures less than 400 °C. The obtained Li-containing particles are nanocrystalline with sizes ranging from 10.9 to 32.9 nm depending on the Li concentrations. PXRD and Raman spectroscopy investigations reveal that Li ions are well incorporated in the MgO lattice if the Li amount reaches up to 1 wt %. The present study demonstrates the usefulness of the single-source precursor (SSP) approach to synthesize Li-containing MgO nanoparticles with varying Li concentrations and high Li ion dispersion.

Experimental Section

General Remarks. All reactions were performed under anaerobic conditions using standard Schlenk techniques. Solvents and alcohols were refluxed over an appropriate drying agent, and distilled and degassed prior to use. [MeMg(μ_3-O^{i}Pr)]$_4$ (**2a**), [MeMg(μ_3-O^{t}Bu)]$_4$ (**2b**), and [MeMg(μ_3-O^{Cy}Hex)]$_4$ (**2c**) were prepared as described previously.[9] All other chemicals were used as received from Merck, Alfa Aesar, or Acros Organics without further purification. Carbon atoms in the cyclohexyl groups are numbered clockwise, beginning at the oxygen atom.

Preparation of [Li(thf)(MeMg)$_3$(μ_3-O^{i}Pr)$_4$] (1a). A solution of 4.30 g (10.9 mmol) of [MeMg (μ_3-O^{i}Pr)]$_4$ and 962 mg (14.6 mmol) of LiO^{i}Pr in 200 mL of THF was stirred for 48 h at room temperature. After filtration, all volatiles were removed in vacuo. Recrystallization from hexane at −20 °C affords **1a** as colorless crystals. Yield: 4.91 g (11.4 mmol; 78%). mp: 288 °C (decomposition) ^{1}H NMR (200 MHz, C_6D_6): δ = 4.08 (sept, J = 6.1 Hz, 1H, −OC$\underline{H}$(CH$_3$)$_2$), 3.93 (sept, J = 6.1 Hz, 3H, −OCH(C$\underline{H}_3$)$_2$), 3.30 (m, 4H, THF), 1.39 (d, J = 6.1 Hz, 6H, −OCH(C$\underline{H}_3$)$_2$), 1.24 (d, J = 6.1 Hz, 18H, −OCH(C$\underline{H}_3$)$_2$), 1.22 (m, 4H, THF), −0.71 ppm (s, 3H, MgC$\underline{H}_3$). ^{13}C{^{1}H}NMR (200 MHz; C_6D_6): δ = 68.1 (THF), 65.0 (−O$\underline{C}$H(CH$_3$)$_2$), 64.0 (−O$\underline{C}$H(CH$_3$)$_2$), 27.6 (−OCH(C$\underline{H}_3$)$_2$), 27.0 (−OCH(C$\underline{H}_3$)$_2$), 24.8 (THF), −15.4 ppm (Mg$\underline{C}$H$_3$). MAS ^{13}C{^{1}H} NMR (100.6 MHz): δ = 69.5 (THF), 64.3 (−O$\underline{C}$H(CH$_3$)$_2$), 63.6 (−O$\underline{C}$H(CH$_3$)$_2$), 27.6 (−OCH(C$\underline{H}_3$)$_2$), 26.8 (−OCH(C$\underline{H}_3$)$_2$), 25.4 (THF), −16.5 ppm (CH$_3$). ^{7}Li{^{1}H} NMR (400 MHz; C_6D_6): δ = −0.06 ppm. MAS ^{7}Li{^{1}H}NMR (400 MHz): δ = 0.35 ppm. $C_{19}H_{45}LiMg_3O_5$ (433.41) Calcd: C, 52.65; H, 10.47. Found: C, 49.68; H, 9.55.

Preparation of [Li(thf)(MeMg)$_3$(μ_3-O^{t}Bu)$_4$] (1b). A solution of 8.00 g (17.8 mmol) of [MeMg (μ_3-O^{t}Bu)]$_4$ and 1.90 g (23.7 mmol) of LiO^{t}Bu in 200 mL THF was stirred for 48 h at room temperature. After filtration, all volatiles were removed in vacuo, and **1b** was isolated as colorless powder. Yield: 8.94 g (18.3 mmol; 77%). mp: 295 °C (decomposition) ^{1}H NMR (200 MHz, C_6D_6): δ = 3.50 (m, 4H, THF), 1.57 (s, 9H, −OC(C$\underline{H}_3$)$_3$), 1.38 (s, 18H, −OC(C$\underline{H}_3$)$_3$), 1.31 (m, 4H, THF), −0.59 ppm (s, 3H, MgCH$_3$). ^{13}C{^{1}H}NMR (200 MHz; C_6D_6): δ = 69.2 (THF), 68.7, 67.8 (C(CH$_3$)$_3$), 33.2, 32.5 (C(C$\underline{H}_3$)$_3$), 25.5 (THF), −11.8 ppm (Mg$\underline{C}$H$_3$). MAS ^{13}C{^{1}H} NMR (400 MHz): δ = 68.2 (THF, C(CH$_3$)$_3$), 32.8 (C(C$\underline{H}_3$)$_3$), 25.0 (THF), −10.5 ppm (CH$_3$). ^{7}Li{^{1}H} NMR (400 MHz; C_6D_6): δ = −0.17 ppm. MAS ^{7}Li{^{1}H} NMR (400 MHz): δ = 0.44 ppm. $C_{23}H_{53}LiMg_3O_5$ (489.52) Calcd: C, 56.43; H, 10.91. Found: C, 55.89; H, 10.57.

Preparation of [Li(thf)(MeMg)$_3$(μ_3-O^{Cy}Hex)$_4$] (1c). A solution of 7.40 g (13.4 mmol) of [MeMg (μ_3-O^{Cy}Hex)]$_4$ and 1.89 g (17.8 mmol) of LiO^{Cy}Hex in 200 mL of THF was stirred for 48 h at room temperature. After filtration, all volatiles were removed in vacuo. Recrystallization from hexane/THF (1:1) at −20 °C affords **1c** as colorless crystals. Yield: 8.70 g (16.6 mmol, 93%). mp: 285 °C (decomp.). ^{1}H NMR (200 MHz; C_6D_6): δ = 3.80, 3.59, 2.48, 2.17, 1.65, 1.50, 1.44, 1.15, 1.10 (m, 48H, −^{Cy}Hex), 3.39 (m, 4H, THF), 1.27 (m, 4H, THF), −0.67 ppm (s, 9H, MgC$\underline{H}_3$). ^{13}C{^{1}H} NMR (200 MHz; C_6D_6): δ = 72.3, 71.7 (^{Cy}Hex(C-1)), 68.7 (THF), 39.2, 38.5 (^{Cy}Hex(C-2)), 25.8, 25.7, 25.6, 25.4, 25.3 (THF; ^{Cy}Hex(C3,C4)), −14.3 ppm (Mg$\underline{C}$H$_3$).). ^{13}C{^{1}H} MAS NMR (400 MHz): δ = 71.5 (−^{Cy}Hex, THF), 38.7 (−^{Cy}Hex), 25.1 (THF; −^{Cy}Hex), −16.0 ppm (−CH$_3$). ^{7}Li{^{1}H} NMR (400 MHz, C_6D_6): δ = 0.07 ppm. MAS ^{7}Li{^{1}H} NMR (400 MHz): δ = 0.7 ppm. $C_{31}H_{61}LiMg_3O_5$ (593.67) Calcd: C, 62.72; H, 10.36. Found: C, 59.71; H, 10.72.

Single-Crystal X-ray Structure Determinations. Crystals were each mounted on a glass capillary in perfluorinated oil and measured in a cold steam of N_2. The data for **1a** and **2b** were collected with a Bruker-AXS SMART CCD diffractometer (Mo Kα radiation, λ = 0.71707 Å, ω-scan). The structures were solved by direct methods. Refinement were carried out with the SHELXL-97 package. All thermal displacement parameters were refined anistropically for non-H atoms and isotropically for H atoms. All refinements were made by full matrix least-squares on F^2. CCDC 764735 contains the supplementary crystallographic data for this paper. These data can be ontained

free of charge via www.ccdc.cam.ac.uk/data_request/cif, by emailing data_requst@ccdc.cam.ac.uk, or by contacting The Cambridge Crystallographic Data Centre, 12, Union Road, Cambridge CB2 1EZ, U.K.; Fax: +44 1223 336033.

Crystal Data for ***1c****:* $C_{31}H_{61}LiMg_3O_5$, M = 593.67; orthorhombic, space group $Pca2_1$; a = 20.1503(6) Å, b = 9.3143(3) Å, c = 19.2849(7) Å; V = 3619.5(2) Å^3; D = 1.089 g cm^{-3}; T = 150 K, 5810 reflections with $I > 2\sigma(I)$, θ_{max} = 25.00°, R1 = 0.0732 (observed reflections), wR2 = 0.1502 (all data) (see also Supporting Information I).

Particle Preparation. Li-doped MgO was prepared by thermolysis of **1a**−**c** or mixtures of **1a** with **1b** in a quartz tube reactor. **1a** and **2** were mixed by dissolving both compounds in THF and subsequent removing the solvent in vacuo. Unless indicated otherwise, the decomposition was carried out in synthetic air (20% O_2, 80% N_2) and the heating rate toward the final temperature (600 °C) was 5 K min^{-1} with a subsequent heating time of 2 h at 600 °C.

Analytical Methods. FT-IR spectra were recorded from KBr pellets by using a Bruker Vektor 22 spectrometer. Powder diffractograms were performed on a Bruker AXS D8 Advance instrument using Cu Kα radiation (λ = 1.5418 Å) and a position sensitive-detector (PSD) in the 2θ range from 25° to 85° with 0.015° step. Crystallite size and microstrain parameters were determined by performing a full profile Warren−Averbach fit of experimental PXRD patterns with subsequent decomposition of reflection profiles into Gaussian and Lorenzian parts, taking into account instrumental contribution to peak broadening. Raman measurements were carried out with the 514 nm excitation line of an Ar+ laser (Innova 300, Coherent) using a confocal Raman microscope (LabRam HR-800, Jobin Yvon). The laser beam was focused on the surface of the working electrode with a long working distance objective (20×; numerical aperture 0.35). Spectral resolution and laser power was 0.9 cm^{-1} and 40 mW, respectively. The accumulation times varied between 30 and 120 s. Elemental analysis was performed on a Perkin-Elmer 2400 CHN-S/O elemental analyzer. Thermogravimetric analysis (TGA) of the precursor was carried out with a thermogravimetric setup from Rubotherm under synthetic air (20% O_2/80% N_2) and with a heating rate of 5 K min^{-1}. The specific BET surface areas were measured using nitrogen adsorption at 77 K with a micromeritics Gemini III 2375 Surface Area Analyzer. Scanning Electron Microscopy (SEM) images were acquired using a Hitachi S-4000 microscope equipped with an SAMX EDX detector located at the ZELMI, TU Berlin. The SEM samples were prepared by shortly dipping a carbon carrier in the solution, where MgO particles were dispersed in acetone. TEM images were recorded on a tecnai G^2 20 S-TWIN with an energy-dispersive X-ray spectrometer (EDAX, r-TEM SUTW) located at the ZELMI, TU Berlin. The solid state MAS (magic angle spinning) NMR measurements were carried out at a Bruker Avance 400 spectrometer operating at 100.6 MHz for ^{13}C and 155.5 MHz for ^7Li using a Bruker 4 mm double-resonance probehead operating at a spinning rate of 10 and 12 kHz for ^{13}C and ^7Li, respectively.

Acknowledgment. We thank the Cluster of Excellence "Unifying Concepts in Catalysis" (sponsored by the Deutsche Forschungsgemeinschaft and admistered by the Technische Universität Berlin) for financial support. We thank also Prof. M. Lehmann and ZELMI (Zentrales Laboratorium für Elektronenmikroskopie, TU Berlin) for TEM analyses, and Inez Weidinger (Insitute of Chemistry, TU Berlin) for Raman spectra and helpful discussions.

Supporting Information Available: Further details on the single-crystal XRD characterization of the precursor **1c**, TGA-DTG (of **1a** and **1c**) and TGA-MS (of **1a**−**c**), the precursor mixtures that were used to prepare Li@MgO samples with different Li content, as well as information concerning the characterization of the prepared Li@MgO samples, such as PXRD, IR-, Raman-, and EDX-spectra for different Li concentrations (PDF). This information is available free of charge via the Internet at http://pubs.acs.org/.